Science Advances

AAAS

advances.sciencemag.org/cgi/content/full/3/1/e1601192/DC1

Supplementary Materials for

Splashing transients of 2D plasmons launched by swift electrons

Xiao Lin, Ido Kaminer, Xihang Shi, Fei Gao, Zhaoju Yang, Zhen Gao, Hrvoje Buljan, John D. Joannopoulos, Marin Soljačić, Hongsheng Chen, Baile Zhang

Published 27 January 2017, *Sci. Adv.* **3**, e1601192 (2017)
DOI: 10.1126/sciadv.1601192

The PDF file includes:

Other Supplementary Material for this manuscript includes the following:
(available at advances.sciencemag.org/cgi/content/full/3/1/e1601192/DC1)

- movie S1 (.mov format). Time evolution of 2D plasmons launched by swift electrons.

section S1. Figure caption of movie S1.

(Left panel) Movie of the spatial-temporal evolution of the magnetic field when a swift electron penetrates through graphene as presented in Fig. 2 in the main text.

(Right panel) Movie of the spatial-temporal evolution of the deviation of the electron density from its average value on graphene when a swift electron penetrates through graphene as presented in Fig. 3 in the main text.

section S2. Photon emission from graphene affected by swift electrons.

In addition to the transition radiation by means of photon emission, the passage of the swift electron through graphene will possibly excite electron-hole pairs, excitons, secondary electrons or Auger electrons. The accompanied decay processes can give rise to the incoherent cathodoluminescence emission or secondary electron emission (*1, 3*), increasing the complexity of this scenario. There is also a small probability for the swift electron to have heavy encounters with graphene atoms, which will generate the so-called bremsstrahlung radiation (*1*). Importantly, these processes can be treated independently from one another for thin enough materials. Moreover, since the coherent cathodoluminescence emission (transition radiation in our case) among electron-induced radiation is dominant in metals (*1*) and doped graphene layer effectively behaves as an ultrathin metallic layer, we treat the transition radiation as the dominant radiation process in this work.

When the frequency is sufficiently below the inter-band threshold, graphene's surface conductivity can be calculated by the local model based on Kubo formula (*30, 31, 39–41*), which agrees well with that calculated by the nonlocal model based on random-phase approximation and number conserving approximation (*25*). When the frequency is below that of the optical phonon branch (surface optical phonons of the substrate (*42*), or intrinsic graphene's phonons (*25*)), the order of magnitude of the relaxation time in Kubo formula can be estimated from the electron mobility. From Kubo formula (*30, 31*), one has

$$\sigma_s(\omega,\mu_c,\tau,T)=\frac{ie^2(\omega+i/\tau)}{\pi\hbar^2}\left[\frac{1}{(\omega+i/\tau)^2}\int_0^{+\infty}E\left(\frac{\partial f_d(E)}{\partial E}-\frac{\partial f_d(-E)}{\partial E}\right)dE-\int_0^{+\infty}\frac{f_d(-E)-f_d(E)}{(\omega+i/\tau)^2-4(E/\hbar)^2}dE\right]$$

where e is the elementary charge, $f_d(E) = (e^{\frac{E-\mu_c}{k_B T}} + 1)^{-1}$ is the Fermi-Dirac distribution, and k_B is the Boltzmann's constant. In this work, we set the temperature $T = 300$ K, the relaxation time $\tau = 0.5$ ps, and the chemical potential in graphene $\mu_c = 0.4$ eV (close to the experimentally achievable value (*32*)).

Within the framework of classical electrodynamics, the current density for a moving charged particle is (*13*, *43*)

$$\bar{J}^q(\bar{r}, t) = \hat{z} q v \delta(x)\delta(y)\delta(z - vt) \tag{1}$$

By decomposing all the quantities in Fourier components in time and in the coordinates $\bar{r}_\perp = \hat{x}x + \hat{y}y$ perpendicular to the moving charge's trajectory, one has

$$\bar{J}^q(\bar{r}, t) = \hat{z} J_z^q(\bar{r}, t) = \hat{z} \int j^q_{\bar{\kappa}_\perp, \omega}(z) e^{i(\bar{\kappa}_\perp \cdot \bar{r}_\perp - \omega t)} d\bar{\kappa}_\perp d\omega \tag{2}$$

$$\bar{E}(\bar{r}, t) = \int \bar{E}_{\bar{\kappa}_\perp, \omega}(z) e^{i(\bar{\kappa}_\perp \cdot \bar{r}_\perp - \omega t)} d\bar{\kappa}_\perp d\omega, \quad \bar{H}(\bar{r}, t) = \int \bar{H}_{\bar{\kappa}_\perp, \omega}(z) e^{i(\bar{\kappa}_\perp \cdot \bar{r}_\perp - \omega t)} d\bar{\kappa}_\perp d\omega \tag{3}$$

where $\bar{\kappa}_\perp = \hat{x}\kappa_x + \hat{y}\kappa_y$. From equations (1–2), one obtains $j^q_{\bar{\kappa}_\perp, \omega}(z) = \frac{q}{(2\pi)^3} e^{i\frac{\omega}{v}z}$. Below we will use mainly the fields (such as $j^q_{\bar{\kappa}_\perp, \omega}$, $\bar{E}_{\bar{\kappa}_\perp, \omega}$ and $\bar{H}_{\bar{\kappa}_\perp, \omega}(z)$) in the Fourier decomposition. For the sake of simplicity, we will not give the indices $\bar{\kappa}_\perp$ and ω for the corresponding Fourier components. By solving Maxwell equations, one can find the following equation for E_z (the component along the charge's trajectory)

$$\frac{\partial^2}{\partial z^2}(\varepsilon_r E_z) + \varepsilon_r \left(\frac{\omega^2}{c^2}\varepsilon_r - \kappa_\perp^2\right) E_z = -\frac{i\omega\mu_0 q}{(2\pi)^3}(\varepsilon_r - \frac{c^2}{v^2}) e^{i\frac{\omega}{v}z} \tag{4}$$

where ε_r is the relative permittivity (i.e. $\varepsilon_r = \varepsilon/\varepsilon_0$, ε_0 is the permittivity of free space), and c is the speed of light in free space. Equation (4) can be solved in each medium, and the solutions should be joined by matching the boundary conditions (*13*, *43*), i.e.

$$\hat{n} \times (\bar{E}_{1\perp} - \bar{E}_{2\perp})|_{z=0} = 0, \quad \hat{n} \times (\bar{H}_{1\perp} - \bar{H}_{2\perp})|_{z=0} = \bar{J}_s = \sigma_s \bar{E}_{1\perp}|_{z=0} \tag{5}$$

where $\hat{n} = -\hat{z}$, $\bar{J}_s$ is the surface current density. Such a solution will be a sum of a field induced by the charge in a homogeneous medium (E_z^q) and the freely radiated field (E_z^R), i.e. $E_z = E_z^q + E_z^R$, where

$$E_z^q = \frac{-iq}{\omega\varepsilon_0(2\pi)^3}\frac{1-\frac{c^2}{v^2\varepsilon_r}}{(\varepsilon_r-\frac{c^2}{v^2}-\frac{\kappa_\perp^2 c^2}{\omega^2})}e^{i\frac{\omega}{v}z} \tag{6}$$

$$E_z^R = \frac{iq}{\omega\varepsilon_0(2\pi)^3}\cdot a\cdot e^{\pm i(\frac{\omega}{c}\sqrt{\varepsilon_r-\frac{\kappa_\perp^2 c^2}{\omega^2}})z} \tag{7}$$

Since the radiated fields should propagate away from the boundary, the $+$ sign is used in the medium 2 in equation (7) and the $-$ sign is used in the medium 1 in equation (7). By matching the boundary conditions, one can obtain the two amplitudes $a_1$and a_2 of the radiation fields in medium 1 and medium 2, i.e.

$$a_1 = \frac{\frac{v}{c}\cdot\frac{\kappa_\perp^2 c^2}{\omega^2\varepsilon_{1r}}(\varepsilon_{2r}-\varepsilon_{1r})[(1-\frac{v^2}{c^2}\varepsilon_{1r}+\frac{v}{c}\sqrt{\varepsilon_{2r}-\frac{\kappa_\perp^2 c^2}{\omega^2}})+\frac{\frac{\sigma_S}{c\varepsilon_0}}{\varepsilon_{2r}-\varepsilon_{1r}}\sqrt{\varepsilon_{2r}-\frac{\kappa_\perp^2 c^2}{\omega^2}}(1+\frac{v}{c}\sqrt{\varepsilon_{2r}-\frac{\kappa_\perp^2 c^2}{\omega^2}})]}{(1-\frac{v^2}{c^2}\varepsilon_{1r}+\frac{\kappa_\perp^2 v^2}{\omega^2})(1+\frac{v}{c}\sqrt{\varepsilon_{2r}-\frac{\kappa_\perp^2 c^2}{\omega^2}})[\varepsilon_{1r}\sqrt{\varepsilon_{2r}-\frac{\kappa_\perp^2 c^2}{\omega^2}}+\varepsilon_{2r}\sqrt{\varepsilon_{1r}-\frac{\kappa_\perp^2 c^2}{\omega^2}}+\frac{\sigma_S}{c\varepsilon_0}\sqrt{\varepsilon_{1r}-\frac{\kappa_\perp^2 c^2}{\omega^2}}\sqrt{\varepsilon_{2r}-\frac{\kappa_\perp^2 c^2}{\omega^2}}]} \tag{8}$$

$$a_2 = \frac{\frac{v}{c}\cdot\frac{\kappa_\perp^2 c^2}{\omega^2\varepsilon_{2r}}(\varepsilon_{2r}-\varepsilon_{1r})[(1-\frac{v^2}{c^2}\varepsilon_{2r}-\frac{v}{c}\sqrt{\varepsilon_{1r}-\frac{\kappa_\perp^2 c^2}{\omega^2}})-\frac{\frac{\sigma_S}{c\varepsilon_0}}{\varepsilon_{2r}-\varepsilon_{1r}}\sqrt{\varepsilon_{1r}-\frac{\kappa_\perp^2 c^2}{\omega^2}}(1-\frac{v}{c}\sqrt{\varepsilon_{1r}-\frac{\kappa_\perp^2 c^2}{\omega^2}})]}{(1-\frac{v^2}{c^2}\varepsilon_{2r}+\frac{\kappa_\perp^2 v^2}{\omega^2})(1-\frac{v}{c}\sqrt{\varepsilon_{1r}-\frac{\kappa_\perp^2 c^2}{\omega^2}})[\varepsilon_{1r}\sqrt{\varepsilon_{2r}-\frac{\kappa_\perp^2 c^2}{\omega^2}}+\varepsilon_{2r}\sqrt{\varepsilon_{1r}-\frac{\kappa_\perp^2 c^2}{\omega^2}}+\frac{\sigma_S}{c\varepsilon_0}\sqrt{\varepsilon_{1r}-\frac{\kappa_\perp^2 c^2}{\omega^2}}\sqrt{\varepsilon_{2r}-\frac{\kappa_\perp^2 c^2}{\omega^2}}]} \tag{9}$$

where ε_{1r} and ε_{2r} are the relative permittivity in medium 1 and medium 2, respectively. In order to investigate transition radiation formed on graphene monolayer , $\varepsilon_{1r}=\varepsilon_{2r}=\varepsilon_r$ is set to facilitate calculation in this work. This way, with the existence of a surface conductivity $\sigma_s \neq 0$, one has $a_1 = -a_2 = a$, where

$$a = \frac{\frac{v}{c}\cdot\frac{\kappa_\perp^2 c^2}{\omega^2\varepsilon_r}\cdot\frac{\sigma_S}{c\varepsilon_0}}{(1-\frac{v^2}{c^2}\varepsilon_r+\frac{\kappa_\perp^2 v^2}{\omega^2})(2\varepsilon_r+\frac{\sigma_S}{c\varepsilon_0}\sqrt{\varepsilon_r-\frac{\kappa_\perp^2 c^2}{\omega^2}})} \tag{10}$$

The above result of equation (3), expressed in the Cartesian coordinates (x, y, z), can also be expressed in the cylindrical coordinates (ρ, ϕ, z). After some calculations, we have

$$\bar{E}_1(\bar{r},t) = \bar{E}_1^q(\bar{r},t) + \bar{E}_1^R(\bar{r},t),\ \bar{H}_1(\bar{r},t) = \bar{H}_1^q(\bar{r},t) + \bar{H}_1^R(\bar{r},t) \tag{11}$$

$$\bar{E}_1^q(\bar{r},t) = \hat{z}\int_{-\infty}^{+\infty} d\omega \frac{-q}{8\pi\omega\varepsilon_0\varepsilon_{1r}}\left(\frac{\omega^2}{c^2}\varepsilon_{1r}-\frac{\omega^2}{v^2}\right)H_0^{(1)}\left(\rho\sqrt{\frac{\omega^2}{c^2}\varepsilon_{1r}-\frac{\omega^2}{v^2}}\right)e^{i\left(\frac{\omega}{v}z-\omega t\right)} +$$

$$\hat{\rho}\int_{-\infty}^{+\infty} d\omega \frac{-q}{8\pi\omega\varepsilon_0\varepsilon_{1r}}(i\frac{\omega}{v})(-\sqrt{\frac{\omega^2}{c^2}\varepsilon_{1r}-\frac{\omega^2}{v^2}}H_1^{(1)}(\rho\sqrt{\frac{\omega^2}{c^2}\varepsilon_{1r}-\frac{\omega^2}{v^2}}))e^{i\left(\frac{\omega}{v}z-\omega t\right)} \tag{12}$$

$$\bar{H}_1^q(\bar{r},t) = \hat{\phi}\int_{-\infty}^{+\infty} d\omega \frac{iq}{8\pi}\sqrt{\frac{\omega^2}{c^2}\varepsilon_{1r}-\frac{\omega^2}{v^2}}H_1^{(1)}(\rho\sqrt{\frac{\omega^2}{c^2}\varepsilon_{1r}-\frac{\omega^2}{v^2}})e^{i\left(\frac{\omega}{v}z-\omega t\right)} \tag{13}$$

$$\bar{E}_1^R(\bar{r},t)=\hat{z}\int_{-\infty}^{+\infty}d\omega\int_0^{+\infty}d\kappa_\perp\cdot\frac{iq}{\omega\varepsilon_0(2\pi)^3}a_1\kappa_\perp\big(2\pi J_0(\kappa_\perp\rho)\big)e^{i[-(\frac{\omega}{c}\sqrt{\varepsilon_{1r}-\frac{\kappa_\perp^2c^2}{\omega^2}})z-\omega t]}+$$

$$\hat{\rho}\int_{-\infty}^{+\infty}d\omega\int_0^{+\infty}d\kappa_\perp\cdot\frac{iq}{\omega\varepsilon_0(2\pi)^3}a_1(\frac{\omega}{c}\sqrt{\varepsilon_{1r}-\frac{\kappa_\perp^2c^2}{\omega^2}})(i2\pi J_1(\kappa_\perp\rho))e^{i[-(\frac{\omega}{c}\sqrt{\varepsilon_{1r}-\frac{\kappa_\perp^2c^2}{\omega^2}})z-\omega t]} \quad (14)$$

$$\bar{H}_1^R(\bar{r},t)=\hat{\phi}\int_{-\infty}^{+\infty}d\omega\int_0^{+\infty}d\kappa_\perp\cdot\frac{iq}{\omega\varepsilon_0(2\pi)^3}a_1(-\omega\varepsilon_{1r}\varepsilon_0)\big(i2\pi J_1(\kappa_\perp\rho)\big)e^{i[-(\frac{\omega}{c}\sqrt{\varepsilon_{1r}-\frac{\kappa_\perp^2c^2}{\omega^2}})z-\omega t]} \quad (15)$$

$$\bar{E}_2(\bar{r},t)=\bar{E}_2^q(\bar{r},t)+\bar{E}_2^R(\bar{r},t),\ \bar{H}_2(\bar{r},t)=\bar{H}_2^q(\bar{r},t)+\bar{H}_2^R(\bar{r},t) \quad (16)$$

$$\bar{E}_2^q(\bar{r},t)=\hat{z}\int_{-\infty}^{+\infty}d\omega\frac{-q}{8\pi\omega\varepsilon_0\varepsilon_{2r}}\left(\frac{\omega^2}{c^2}\varepsilon_{2r}-\frac{\omega^2}{v^2}\right)H_0^{(1)}\left(\rho\sqrt{\frac{\omega^2}{c^2}\varepsilon_{2r}-\frac{\omega^2}{v^2}}\right)e^{i\left(\frac{\omega}{v}z-\omega t\right)}+$$

$$\hat{\rho}\int_{-\infty}^{+\infty}d\omega\frac{-q}{8\pi\omega\varepsilon_0\varepsilon_{2r}}(i\frac{\omega}{v})(-\sqrt{\frac{\omega^2}{c^2}\varepsilon_{2r}-\frac{\omega^2}{v^2}}H_1^{(1)}(\rho\sqrt{\frac{\omega^2}{c^2}\varepsilon_{2r}-\frac{\omega^2}{v^2}}))e^{i\left(\frac{\omega}{v}z-\omega t\right)} \quad (17)$$

$$\bar{H}_2^q(\bar{r},t)=\hat{\phi}\int_{-\infty}^{+\infty}d\omega\frac{iq}{8\pi}\sqrt{\frac{\omega^2}{c^2}\varepsilon_{2r}-\frac{\omega^2}{v^2}}H_1^{(1)}(\rho\sqrt{\frac{\omega^2}{c^2}\varepsilon_{2r}-\frac{\omega^2}{v^2}})e^{i\left(\frac{\omega}{v}z-\omega t\right)} \quad (18)$$

$$\bar{E}_2^R(\bar{r},t)=\hat{z}\int_{-\infty}^{+\infty}d\omega\int_0^{+\infty}d\kappa_\perp\cdot\frac{iq}{\omega\varepsilon_0(2\pi)^3}a_2\kappa_\perp\big(2\pi J_0(\kappa_\perp\rho)\big)e^{i[+(\frac{\omega}{c}\sqrt{\varepsilon_{2r}-\frac{\kappa_\perp^2c^2}{\omega^2}})z-\omega t]}+$$

$$\hat{\rho}\int_{-\infty}^{+\infty}d\omega\int_0^{+\infty}d\kappa_\perp\cdot\frac{iq}{\omega\varepsilon_0(2\pi)^3}a_2(-\frac{\omega}{c}\sqrt{\varepsilon_{2r}-\frac{\kappa_\perp^2c^2}{\omega^2}})(i2\pi J_1(\kappa_\perp\rho))e^{i[+(\frac{\omega}{c}\sqrt{\varepsilon_{2r}-\frac{\kappa_\perp^2c^2}{\omega^2}})z-\omega t]} \quad (19)$$

$$\bar{H}_2^R(\bar{r},t)=\hat{\phi}\int_{-\infty}^{+\infty}d\omega\int_0^{+\infty}d\kappa_\perp\cdot\frac{iq}{\omega\varepsilon_0(2\pi)^3}a_2(-\omega\varepsilon_{2r}\varepsilon_0)\big(i2\pi J_1(\kappa_\perp\rho)\big)e^{i[+(\frac{\omega}{c}\sqrt{\varepsilon_{2r}-\frac{\kappa_\perp^2c^2}{\omega^2}})z-\omega t]} \quad (20)$$

By enforcing the boundary conditions, one can further have the induced surface charge density $\rho_s(\bar{r},t)$, i.e.

$$\rho_s(\bar{r},t)=\hat{n}\cdot(\varepsilon_1\bar{E}_1(\bar{r},t)-\varepsilon_2\bar{E}_2(\bar{r},t)) \quad (21)$$

This way, the time evolution of the deviation of the electron density from its average value on graphene, $\delta n(\bar{r},t)=-\rho_s(\bar{r},t)/e$, can be numerically calculated, as shown in Fig. 3 in the main text.

section S3. Energy spectrum of induced charges on graphene.

Due to the comparatively negligible energy of transition radiation of light, the total effective electromagnetic "energy" W(t) maintained on graphene (excluding the electron field) is $W(\mathrm{t}) = \int_0^\infty d\omega \cdot W^s(\omega, t)$, where $W^s(\omega, t)$ is the spectrum of induced charge fields. Note that graphene plasmons have not been generated before their formation times. So this "energy" should be considered as a parameter related to the field strength, but not the real energy. Only after $t > L_{f2}/v$ can $W^s(\omega, t)$ represent the real energy of generated graphene plasmons with frequency ω. By integrating the electric and magnetic energies over the whole space (*44*, *45*), one has

$$W(\mathrm{t}) = \int d\omega \iiint dxdydz \int d\omega' \frac{1}{2}[Re\left(\frac{\omega\varepsilon_z(z,\omega)-\omega'\varepsilon_z(z,-\omega')}{\omega-\omega'}\right)\bar{E}_z^R(\bar{r},\omega)\bar{E}_z^R(\bar{r},-\omega')e^{-i(\omega-\omega')t} + Re\left(\frac{\omega\varepsilon_\perp(z,\omega)-\omega'\varepsilon_\perp(z,-\omega')}{\omega-\omega'}\right)\bar{E}_\perp^R(\bar{r},\omega)\bar{E}_\perp^R(\bar{r},-\omega')e^{-i(\omega-\omega')t} + \mu_0\bar{H}_\perp^R(\bar{r},\omega)\bar{H}_\perp^R(\bar{r},-\omega')e^{-i(\omega-\omega')t}] \quad (22)$$

Here the permittivity $\varepsilon(z) = \varepsilon_1(z<0) + \varepsilon_{gra}(z=0) + \varepsilon_2(z>0)$ is *z*-dependent, $\varepsilon_{gra}$is the effective permittivity of uniaxial graphene, where the component $\varepsilon_{gra,\perp} = \frac{i\sigma_s}{\omega}\delta(z)$. After numerically obtaining $\bar{E}^R(\bar{r},\omega)$ and $\bar{H}^R(\bar{r},\omega)$, one can further numerically obtain the time-dependent $W^s(\omega, t)$.

section S4. Dispersion relation and propagation length/time of graphene plasmons.

Dispersion relation for transverse magnetic (TM) graphene plasmons is analytically obtained as

$$\varepsilon_{1r}\sqrt{\varepsilon_{2r}-\frac{\kappa_\perp^2c^2}{\omega^2}} + \varepsilon_{2r}\sqrt{\varepsilon_{1r}-\frac{\kappa_\perp^2c^2}{\omega^2}} + \frac{\sigma_s}{c\varepsilon_0}\sqrt{\varepsilon_{1r}-\frac{\kappa_\perp^2c^2}{\omega^2}}\sqrt{\varepsilon_{2r}-\frac{\kappa_\perp^2c^2}{\omega^2}} = 0 \quad (23)$$

When $\varepsilon_{1r} = \varepsilon_{2r} = \varepsilon_r$ and $\sigma_s \neq 0$, one has

$$2\varepsilon_r + \frac{\sigma_s}{c\varepsilon_0}\sqrt{\varepsilon_r-\frac{\kappa_\perp^2c^2}{\omega^2}} = 0 \quad (24)$$

The dispersion relation of TM graphene plasmons is shown in fig. S1. We also note that graphene plasmons exhibit a typical dispersion of 2D plasmon oscillations, i.e. $\omega \propto \sqrt{\kappa_\perp}$ (*24*, *46*),

similar to the dispersion of hydrodynamic deep-water-waves (*47*). The propagation time, defined as the ratio between propagation length and the group velocity of graphene plasmons, is shown in fig. S2. The propagation length $\frac{1}{2Im(\kappa_\perp)}$ is defined as the distance for the intensity of graphene plasmons to decay by a factor of e^{-1}.

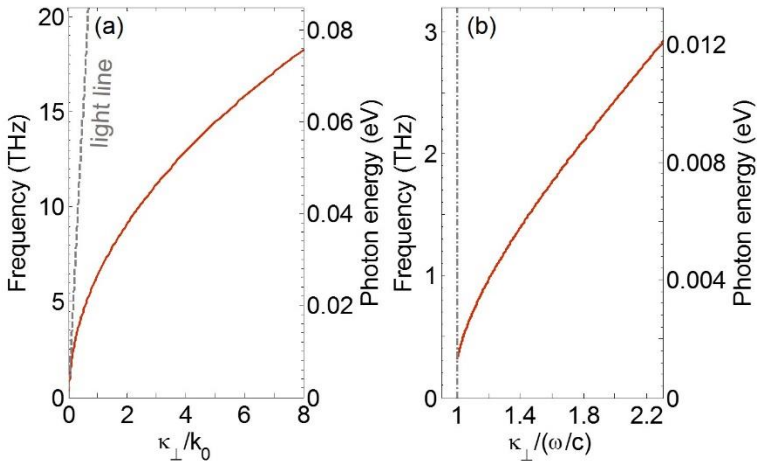

fig. S1. Dispersion curve of TM graphene plasmons. Here we set $\varepsilon_r = 1$, the chemical potential $\mu_c = 0.4$ eV and the relaxation time $\tau = 0.5$ ps. (**A**) The horizontal axis is the wave propagation vector $\kappa_\perp$ normalized by $k_0 = \frac{2\pi}{\lambda_0}$, where $\lambda_0 = 10$ μm. Since the group velocity is $v_g = \frac{\partial\omega}{\partial\kappa_\perp}$, graphene plasmons with longer wavelength have larger group velocities. (**B**) The horizontal axis is $\kappa_\perp$ normalized by $\frac{\omega}{c}$. Due to the existence of loss in graphene, the mode of graphene plasmon disappears below 0.3 THz.

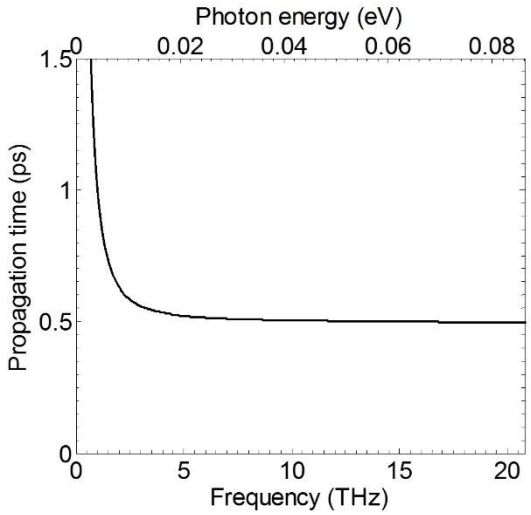

fig. S2. Propagation time of TM graphene plasmons as a function of frequency. Parameter settings are same with that in fig. S2.

section S5. Analytical EEL spectrum.

Our EEL spectrum calculation here, as is typical with EEL spectrum calculations, assumes the electron current is low enough so that the electrons are well-separated from one another. Therefore, there is negligible interaction between these electrons. This assumption matches the relevant currents in transmission electron microscopes. Much higher electron densities (e.g., pulsed operation) can cause interference between the fields emitted by different electrons. Even then, the emitted fields, EEL spectrum and the energy dissipation before 2D plasmons are generated can still be obtained through the theory presented in this work. Needless to say, more researches will be required in cases where the resulting field amplitude is high enough to require considering the nonlinear optical response of graphene.

We neglect the loss in all media in this part. The energy loss from the swift electron will eventually convert to electromagnetic energy of graphene plasmons after a long time. Thus the electromagnetic energy of graphene plasmons W^s can be expressed as (*13, 44*)

$$W^s = \lim_{t\to\infty} \int d\bar{r}_\perp \int_{-\infty}^{\infty} dz \int_{-\infty}^{t} \left(\bar{E}_z^R(\bar{r},t') \cdot \frac{\partial}{\partial t'} \bar{D}_z^R(\bar{r},t') + \bar{E}_\perp^R(\bar{r},t') \cdot \frac{\partial}{\partial t'} \bar{D}_\perp^R(\bar{r},t') + \bar{H}_\perp^R(\bar{r},t') \cdot \frac{\partial}{\partial t'} \bar{B}_\perp^R(\bar{r},t') \right) dt' \qquad (25)$$

Here we have used the fact that $\bar{H}_z^R = 0$. Substituting equation (3) into equation (25) and symmetrizing the result by means of the replacement $\omega \leftrightarrows -\omega'$and $\bar{\kappa}_\perp \leftrightarrows -\bar{\kappa}_\perp'$ (*13*, *44*), one has

$$W^s = \lim_{t\to\infty} 2\pi^2\{\int_{-\infty}^{\infty} dz \int_{-\infty}^{\infty} d\omega d\omega' \int d\bar{\kappa}_\perp e^{-i(\omega-\omega')t}[\frac{\omega\varepsilon_z(z,\omega)-\omega'\varepsilon_z(z,-\omega')}{\omega-\omega'} E^R_{z,\omega,\bar{\kappa}_\perp}(z)E^R_{z,-\omega',-\bar{\kappa}_\perp}(z) +$$

$$\frac{\omega\varepsilon_\perp(z,\omega)-\omega'\varepsilon_\perp(z,-\omega')}{\omega-\omega'} \bar{E}^R_{\perp,\omega,\bar{\kappa}_\perp}(z)\cdot\bar{E}^R_{\perp,-\omega',-\bar{\kappa}_\perp}(z) + \frac{\omega\mu(z,\omega)-\omega'\mu(z,-\omega')}{\omega-\omega'} \bar{H}^R_{\perp,\omega,\bar{\kappa}_\perp}(z)\cdot\bar{H}^R_{\perp,-\omega',-\bar{\kappa}_\perp}(z)]\} \quad (26)$$

The permittivity $\varepsilon(z) = \varepsilon_1(z<0) + \varepsilon_{gra}(z=0) + \varepsilon_2(z>0)$ is z dependent. Graphene is a uniaxial medium, where the component $\varepsilon_{gra,\perp} = \frac{i\sigma_s}{\omega}\delta(z)$. When $\omega' \to \omega$, $\frac{\omega\varepsilon(z,\omega)-\omega'\varepsilon(z,-\omega')}{\omega-\omega'}$ and $\frac{\omega\mu(z,\omega)-\omega'\mu(z,-\omega')}{\omega-\omega'}$ tend to $\frac{\partial\omega\varepsilon(\omega)}{\partial\omega}$ and $\frac{\partial\omega\mu(\omega)}{\partial\omega}$, respectively. In this work, we set the relative permeability $\mu_{1r} = \mu_{2r} = 1$. In equation (26), the energy for $\omega' \neq \omega$ oscillates rapidly with time, and for $t \to \infty$ only the terms corresponding to $\omega' = \omega$ should be kept (*13*). The integration of z gives three parts of energy, which are below, within and above graphene layer, respectively. When integrating *z* to obtain the field energy within graphene layer, due to the appearance of $\delta(z)$, only the field component parallel to graphene plane will make a contribution and the term related to $\varepsilon_{gra,\perp}(\omega)$ will become to $\frac{i\sigma_s(\omega)}{\omega}$. According to equations (23), one can denote the quantity $\bar{\zeta}_{\omega,\kappa_\perp}$ as

$$\bar{\zeta}_{\omega,\kappa_\perp} = \varepsilon_{1r}\sqrt{\frac{\kappa_\perp^2c^2}{\omega^2}-\varepsilon_{2r}} + \varepsilon_{2r}\sqrt{\frac{\kappa_\perp^2c^2}{\omega^2}-\varepsilon_{1r}} + \frac{i\sigma_s}{c\varepsilon_0}\frac{\omega}{|\omega|}\sqrt{\frac{\kappa_\perp^2c^2}{\omega^2}-\varepsilon_{1r}}\sqrt{\frac{\kappa_\perp^2c^2}{\omega^2}-\varepsilon_{2r}} \quad (27)$$

Then one can include the quantity $\bar{\zeta}_{\omega,\kappa_\perp}$ in the amplitudes a_1 and a_2

$$a_2 = -i\frac{\omega}{|\omega|}\frac{1}{\bar{\zeta}_{\omega,\kappa_\perp}}b_{2,\omega,\kappa_\perp}, \qquad a_1 = -i\frac{\omega}{|\omega|}\frac{1}{\bar{\zeta}_{\omega,\kappa_\perp}}b_{1,\omega,\kappa_\perp} \quad (28)$$

When $\varepsilon_{1r} = \varepsilon_{2r} = \varepsilon_r$ and $\sigma_s \neq 0$, we have $a_1 = -a_2 = a$, $\bar{\zeta}_{\omega,\kappa_\perp} = 2\varepsilon_r + \frac{i\sigma_s}{c\varepsilon_0}\frac{\omega}{|\omega|}\sqrt{\frac{\kappa_\perp^2c^2}{\omega^2}-\varepsilon_r}$, and $b_{\omega,\kappa_\perp} = b_{1,\omega,\kappa_\perp} = -b_{2,\omega,\kappa_\perp} = \frac{\frac{v}{c}\cdot\frac{\kappa_\perp^2c^2}{\omega^2\varepsilon_r}\cdot\frac{\sigma_s}{c\varepsilon_0}}{(1-\frac{v^2}{c^2}\varepsilon_r+\frac{\kappa_\perp^2v^2}{\omega^2})}$. After some algebra, the energy W^s can be written in terms of $b_{\omega,\kappa_\perp}$

$$W^s = \lim_{t\to\infty}\frac{q^2}{32\pi^3\varepsilon_0}\int_0^\infty d\kappa_\perp^2\int_{-\infty}^{\infty} d\omega\int_{-\infty}^{\infty} d\omega'\frac{e^{-i(\omega-\omega')t}}{\bar{\zeta}_{\omega,\kappa_\perp}\bar{\zeta}_{-\omega',\kappa_\perp}}\frac{|b_{\omega,\kappa_\perp}|^2}{\omega^2}\{\frac{\frac{\partial[\omega\varepsilon_r(\omega)]}{\partial\omega}\left(2-\frac{\varepsilon_r(\omega)\omega^2}{\kappa_\perp^2c^2}\right)+\frac{\omega^2\varepsilon_r^2(\omega)}{\kappa_\perp^2c^2}}{\sqrt{\kappa_\perp^2-\frac{\omega^2}{c^2}\varepsilon_r(\omega)}} + \frac{\partial\left[\frac{i\sigma_s(\omega)}{\varepsilon_0}\right]}{\partial\omega}\frac{\omega^2}{\kappa_\perp^2c^2}(\frac{\kappa_\perp^2c^2}{\omega^2}-\varepsilon_r(\omega))\} \quad (29)$$

where the term in the brace is even with respect to ω and $\kappa_\perp$. For even function $\varphi(\omega) = \varphi(-\omega)$, one has

$$\lim_{t\to\infty} \int_{-\infty}^{\infty} d\omega\varphi(\omega) \int_{-\infty}^{\infty} d\omega' \frac{e^{-i(\omega-\omega')t}}{\bar{\zeta}_{\omega,\kappa_\perp}\bar{\zeta}_{-\omega',\kappa_\perp}} = 8\pi^2 \int_0^{\infty} d\omega\varphi(\omega) \frac{\delta(\bar{\zeta}_{\omega,\kappa_\perp})}{(\partial/\partial\omega)\bar{\zeta}_{\omega,\kappa_\perp}} \tag{30}$$

By substituting equation (30) into equation (29), one has

$$W^s = \frac{q^2}{4\pi\varepsilon_0} \int_0^{\infty} \frac{d\omega}{\omega^2} \int_0^{\infty} d\kappa_\perp^2 \frac{|b_{\omega,\kappa_\perp}|^2 \delta(\bar{\zeta}_{\omega,\kappa_\perp})}{(\partial/\partial\omega)\bar{\zeta}_{\omega,\kappa_\perp}} \frac{\frac{\partial[\omega\varepsilon_r(\omega)]}{\partial\omega}\left(2-\frac{\varepsilon_r(\omega)\omega^2}{\kappa_\perp^2 c^2}\right)+\frac{\omega^2\varepsilon_r^2(\omega)}{\kappa_\perp^2 c^2}}{\sqrt{\kappa_\perp^2-\frac{\omega^2}{c^2}\varepsilon_r(\omega)}} \tag{31}$$

When $\omega > 0$, the equation $\bar{\zeta}_{\omega,\kappa_\perp} = 0$ has only one solution for κ^2. By integrating over $d\kappa_\perp^2$ in equation (31) and expressing $W^s = \int_0^{\infty} W^s(\omega)d\omega$, one can have the energy spectrum of graphene plasmons

$$W^s(\omega) = \frac{q^2\varepsilon_r}{\pi\varepsilon_0 c} \frac{\frac{v^2}{c^2}|\frac{\sigma_s}{\varepsilon_0 c}-4\varepsilon_r\frac{\varepsilon_0 c}{\sigma_s}|^2}{[1-\frac{v^2}{c^2}(\frac{2\varepsilon_r\varepsilon_0 c}{\sigma_s})^2]^2} \cdot \frac{1}{-\frac{i\sigma_s}{\varepsilon_0 c}[2\varepsilon_r-\frac{1}{2}(\frac{\sigma_s}{\varepsilon_0 c})^2]} \tag{32}$$

When $\varepsilon_r = 1$, equation (32) reduces to $W^s(\omega) = \frac{q^2}{\pi\varepsilon_0 c} \frac{\frac{v^2}{c^2}|\frac{\sigma_s}{\varepsilon_0 c}-4\frac{\varepsilon_0 c}{\sigma_s}|^2}{[1-\frac{v^2}{c^2}(\frac{2\varepsilon_0 c}{\sigma_s})^2]^2} \cdot \frac{1}{-\frac{i\sigma_s}{\varepsilon_0 c}[2-\frac{1}{2}(\frac{\sigma_s}{\varepsilon_0 c})^2]}$. Because the energy of emitted photons is much smaller than the energy of graphene plasmons, we can safely regard the energy of surface plasmons as the energy loss of the incident electron. This way, one has the loss probability of losing energy $\hbar\omega$ when an electron perpendicularly crossing the interface as

$$\Gamma_\perp(\omega) = W^s(\omega)/(\hbar\omega) \tag{33}$$

For the case with $\sigma_s \neq 1$ and $\varepsilon_{2r} = \varepsilon_{1r} = 1$, according to equation (32), one has

$$\Gamma_\perp(\omega) = \frac{q^2}{\hbar\omega\pi\varepsilon_0 c} \frac{\frac{v^2}{c^2}|\frac{\sigma_s}{\varepsilon_0 c}-4\frac{\varepsilon_0 c}{\sigma_s}|^2}{[1-\frac{v^2}{c^2}(\frac{2\varepsilon_0 c}{\sigma_s})^2]^2} \cdot \frac{1}{-\frac{i\sigma_s}{\varepsilon_0 c}[2-\frac{1}{2}(\frac{\sigma_s}{\varepsilon_0 c})^2]} \tag{34}$$

When $v = 0.8c$, we have plotted $\Gamma_\perp(\omega)$ in fig. S3. When the frequency is above 20 THz, $\Gamma_\perp(\omega)$ approximately goes to zero. This indicates that it is reasonable to set the bandwidth of numerical calculation to be 0 to 20 THz. Moreover, since the onset of optical phonon is 0.2 eV

(corresponding to ~48 THz), the contribution from the optical phonon to the relaxation time can be safely neglected in the calculation.

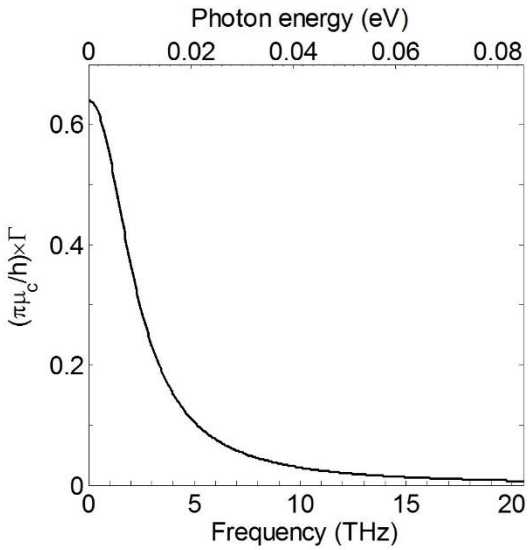

fig. S3. EEL spectrum when an electron normally incident on an ideal lossless graphene layer. Here the electron energy loss spectrum $\Gamma_\perp(\omega)$ is calculated based on equation (34). The velocity of the swift electron is v = 0.8c. When the frequency is above 20 THz, $\Gamma_\perp(\omega)$ approximately goes to zero.

section S6. Comparison of EEL spectra between previous work and our result.

The loss probability $\Gamma_\perp(\omega)$ in equation (6) of Ref. [1] can be deduced from our equation (34) under electrostatic approximation. Same with Ref. [1], one can characterize graphene's surface conductivity by Drude model. In the limit of $\omega\tau \gg 1$ (assuming trivial loss in graphene), one has $\sigma_s \approx \frac{e^2 E_F}{\pi\hbar^2}\frac{i}{\omega}$. This way, equation (34) becomes $\Gamma_\perp(\omega) = \frac{2\hbar}{E_F}\frac{(s^2+\frac{v^2}{c^2})}{(1+s^2)^2}$, where $s = \frac{1}{2\alpha}\frac{v}{c}\frac{\hbar\omega}{\mu_c}$ and $\alpha = \frac{e^2}{4\pi\varepsilon_0\hbar c}$. Under the condition of $s \gg v/c$ or $\frac{1}{2\alpha}\frac{\hbar\omega}{E_F} \gg 1$ (i.e. the electrostatic approximation in Ref. [1]), we have

$$\Gamma_\perp(\omega) \approx \frac{2\hbar}{E_F}\frac{s^2}{(1+s^2)^2} \tag{35}$$

which is exactly the equation (6) of $\Gamma_{\perp}(\omega)$ in Ref. [1]. The comparison of $\Gamma_{\perp}(\omega)$ between this work and Ref. [1] under different electron kinetic energies is shown in fig. S4, where previous $\Gamma_{\perp}(\omega)$ in Ref. [1] is found not applicable for cases with high electron kinetic energies. This is because when the incident electron's kinetic energy is high, the electrostatic approximation in Ref. [1] is no longer valid.

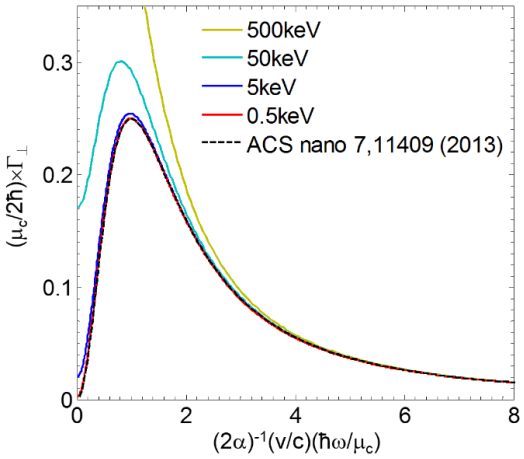

fig. S4. EEL spectra for an electron normally incident on graphene. For comparison with Ref. [1], graphene is characterized by Drude model with $\mu_c = 0.5$ eV. The black dashed line is drawn based on equation (6) in Ref. [1] (or equation (35) below) under the electrostatic approximation, which is independent of the electron kinetic energy. Other lines are drawn based on our equation (34) without the electrostatic approximation. Electron kinetic energies of 0.5keV, 5keV, 50keV and 500keV correspond to electron velocities of 0.044c, 0.14c, 0.41c and 0.83c, respectively.

section S7. Total energy of emitted photons.

One can calculate the total energy W_1 radiated by the charged particle into the medium 1, i.e. backwards relative to its motion, by integrating the radiation field energy density over all space. For long time t, the radiated wave-train is already at a great distance to the boundary and then separated from the charge's intrinsic field. If the origin is moved along the axis into the region of the radiated wave-train, the integration with respect to z can be taken from $-\infty$ to $+\infty$, since the field is attenuated in both directions (*45*).

For freely propagating waves, since the electric and magnetic energy densities are equal, we have

$$W_1 = \int dxdy \int_{-\infty}^{+\infty} dz \cdot \varepsilon_1 |\bar{E}_1^R(\bar{r},t)|^2 \tag{36}$$

$$|\bar{E}_1^R(\bar{r},t)|^2 = \int \bar{E}_{1|\bar{\kappa}_\perp,\omega}^R(z) \cdot \bar{E}_{1|\bar{\kappa}_\perp^{'},\omega^{'}}^{R\ *}(z) e^{i[(\bar{\kappa}_\perp - \bar{\kappa}_\perp^{'})\cdot\bar{r}_\perp - (\omega-\omega^{'})t]}\, d\bar{\kappa}_\perp d\bar{\kappa}_\perp^{'} d\omega d\omega^{'} \tag{37}$$

Substituting equation (37) into equation (36) and integrating over $dxdyd\bar{\kappa}_\perp^{'}\ dzd\omega^{'}$ in equation (36) gives

$$W_1 = 2\int_0^{+\infty} \int \varepsilon_1 |a_1|^2 \left(\frac{q}{\omega\varepsilon_0(2\pi)^3}\right)^2 \frac{\omega^2}{c\kappa_\perp^2} \sqrt{\varepsilon_{1r}} \sqrt{1 - \frac{\kappa_\perp^2 c^2}{\omega^2 \varepsilon_{1r}}} (2\pi)^3 d\bar{\kappa}_\perp d\omega \tag{38}$$

For emitted photons, the integration over $d\bar{\kappa}_\perp$ is to be taken over the range $\kappa_\perp^2 < \frac{\omega^2}{c^2}\varepsilon_{1r}$. We use the angle θ between the radiation wave vector $\bar{k}_1 = (\bar{\kappa}_\perp, \hat{z}k_{1z})$ and the direction of the vector $-\bar{v}$, so that $\theta = 0$ represents radiation in the opposite direction of the particle's motion. Then we can express $\kappa_\perp = \frac{\omega}{c}\sqrt{\varepsilon_{1r}} sin\theta$. A further change from integration over $d\bar{\kappa}_\perp$ to one over $2\pi\kappa_\perp d\kappa_\perp = 2\pi(\frac{\omega^2}{c^2}\varepsilon_{1r}) sin\theta cos\theta d\theta$ in equation (38) gives

$$W_1 = \int_0^{+\infty} \int_0^{\pi/2} U_1(\omega,\theta) \cdot (2\pi sin\theta) d\theta\, d\omega \tag{39}$$

The function $U_1(\omega,\theta) = \frac{\varepsilon_{1r}^{3/2} q^2 cos^2\theta}{4\pi^3 \varepsilon_0 c sin^2\theta} |a_1|^2$ is the angular spectral energy density, which shows the distribution of the radiation in frequency and angle (*45*). With a_1 from equation (8), one finally has

$$U_1(\omega,\theta) = \frac{\sqrt{\varepsilon_{1r}} q^2 \beta^2 cos^2\theta sin^2\theta}{4\pi^3 \varepsilon_0 c(1-\varepsilon_{1r}\beta^2 cos^2\theta)^2} \left| \frac{(\varepsilon_{2r}-\varepsilon_{1r})[(1-\beta^2\varepsilon_{1r}+\beta\sqrt{\varepsilon_{2r}-\varepsilon_{1r}sin^2\theta}) + \frac{\frac{\sigma_S}{c\varepsilon_0}}{\varepsilon_{2r}-\varepsilon_{1r}}\sqrt{\varepsilon_{2r}-\varepsilon_{1r}sin^2\theta}(1+\beta\sqrt{\varepsilon_{2r}-\varepsilon_{1r}sin^2\theta})]}{(1+\beta\sqrt{\varepsilon_{2r}-\varepsilon_{1r}sin^2\theta})[\sqrt{\varepsilon_{1r}}\sqrt{\varepsilon_{2r}-\varepsilon_{1r}sin^2\theta} + \varepsilon_{2r}cos\theta + \frac{\sigma_S}{c\varepsilon_0}cos\theta\sqrt{\varepsilon_{2r}-\varepsilon_{1r}sin^2\theta}]} \right|^2 \tag{40}$$

When $\sigma_s = 0$, the equation (40) is referred as the Ginzburg-Frank formula in the literature (*13*, *45*). When $\varepsilon_{1r} = \varepsilon_{2r} = \varepsilon_r$ and $\sigma_s \neq 0$, with a_1 from equation (10), we obtain

$$U_1(\omega,\theta) = \frac{\sqrt{\varepsilon_r} q^2 \beta^2 cos^2\theta sin^2\theta}{4\pi^3 \varepsilon_0 c(1-\varepsilon_r\beta^2 cos^2\theta)^2} \left| \frac{\frac{\sigma_S}{c\varepsilon_0}}{2\sqrt{\varepsilon_r} + \frac{\sigma_S}{c\varepsilon_0}cos\theta} \right|^2 \tag{41}$$

By expressing the total energy as $W_1 = \int_0^\infty W_1(\omega)d\omega$, one has the energy spectrum of backward radiation as

$$W_1(\omega) = \int_0^{\pi/2} U_1(\omega,\theta)\cdot(2\pi sin\theta)d\theta \tag{42}$$

Following the above calculation procedure, we also obtain the energy spectrum of forward radiation, i.e. $W_2(\omega)$. The total emitted photon spectrum thus is $W(\omega)$=$W_1(\omega) + W_2(\omega)$. The total energy of emitted photons can be obtained by integrating over frequency.

section S8. Numerical implementation with Sommerfeld integration.

By choosing the Sommerfeld branch cut and using the Sommerfeld integration path (*48*, *49*), numerical integration of equation (3) can be carried out. For the numerical integration of fields in Figs. 2–3 in the main text, we treat the current density in equation (1) having a Gaussian-shape space dependence

$$\bar{J}_G^q(\bar{r},t) = \hat{z}qv\delta(x)\delta(y)\frac{1}{\sigma_z\sqrt{2\pi}}e^{-\frac{(z-vt)^2}{2\sigma_z^2}} \tag{43}$$

where this kind of Gaussian-shape electron bunching has been used to study the Cherenkov radiation (*50–52*). Then the amplitude a of transition radiation in equation (10) changes accordingly, i.e. $a_G = ae^{-\frac{\sigma_z^2}{2}\cdot\frac{\omega^2}{v^2}}$. When $\sigma_z = 0$, the current density returns to $\bar{J}_G^q(\bar{r},t) = \bar{J}^q(\bar{r},t) = \hat{z}qv\delta(x)\delta(y)\delta(z-vt)$ and $a_G = a$. In Figs. 2–3 in the main text, we set $\sigma_z = 5$ μm and integrate the frequency from 0 to 20 THz.